OSCILLATION MECHANISMS OF LASER-SUSTAINED PLASMA: A KEY TO STABILIZING LIGHT SOURCES FOR WAFER DEFECT INSPECTION

Dongheyu Zhang[1], and Yangyang Fu[1]*
[1]Department of Electrical Engineering, Tsinghua University, Beijing, China
*Corresponding Author's Email: fuyangyang@tsinghua.edu.cn

ABSTRACT

Laser-sustained plasma (LSP) is a high-temperature, high-radiation plasma widely used in semiconductor wafer inspection. However, the mechanisms of its brightness instability remain mysterious and strongly impede the development of ultra-broadband stabilized light sources. In this work, we elucidate that the LSP oscillation behaviors stem from buoyancy-driven vortex dynamics through the high-speed shadow image and an advanced multi-physics fluid model. A vorticity-resolved scaling law for LSP oscillation frequency, incorporating the gas properties and gravitational acceleration, is proposed for the first time. The generalized scaling law enables predictive control of LSP stability, enhancing the precision of high-resolution wafer optical inspection.

INTRODUCTION

Laser-sustained plasma (LSP), also termed as continuous optical discharge (COD), is a type of high energy density thermal plasma maintained by focused continuous wave (CW) laser radiation in high-pressure gases [1-2]. LSP has a variety of outstanding features, including high temperature, high degree of ionization, and high radiance over a broad spectral range, which attracts increasing attention as a novel broadband light source for next generation fore-end wafer defect inspection. Despite its many advantages, the generation and depression of illumination instability in LSP remains unclear [3-4].

In this work, by combining high-speed shadow image visualization, photodetector measurements, and the corresponding simulation results, it is fully determined that LSP's unstable brightness is essentially caused by the formation, development and detachment of vortices around the LSP core. Furthermore, for the first time, a generalized scaling law for LSP oscillation frequency f_{os} is proposed by dimensional analysis, fully incorporating the gas properties (heat capacity C_p, thermal conductivity k_T, and gas density ρ) and gravitational acceleration g via dimensional analysis, which is validated by simulation and experimental results. These advancements facilitate predictive modeling of LSP stability, a prerequisite for high-precision semiconductor manufacturing.

METHODS

Experimental Setup

As shown in Fig. 1(a), LSP is ignited in a xenon-filled bulb (10 atm) by a high-voltage pulse (~20 kV, ~25 ns). The plasma is maintained by a CW 1080 nm fiber laser focused to an intensity of 10^{10}-10^{11} W/m^2. Input and transmitted laser powers are measured with a thermal laser power meter. A time-resolved shadowgraph system is used to visualize the density distribution around the LSP. A 532 nm laser provides collimated backlight, and a lens and camera assembly records the shadow images. Refractive-index gradients in the images reflect density variations in the gas flow. The oscillation frequency of the flow field is extracted from high-speed shadow sequences. Additionally, plasma emission fluctuations are recorded with a photodetector and oscilloscope, and the brightness oscillation frequency is obtained via fast Fourier transform (FFT) of the temporal signal.

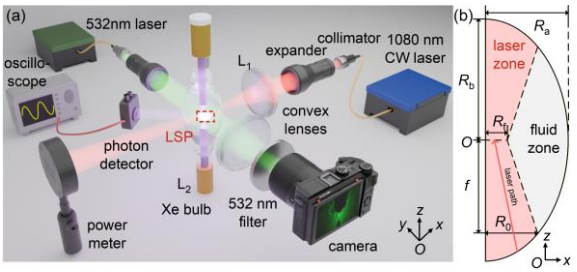

Figure 1: (a) The global view of the shadowgraph diagnosis system. (b) Computational domain of the 2D symmetric cylindrical xoz coordinates of the model [6].

Multiphysics Simulation Model

A 2D multiphysics model is established to simulate the oscillation behavior of the LSP, and the details are provided in our previous works [1,5]. The computational domain is a semi-elliptical shaped region matching the experimental bulb dimensions [Fig. 1(b)]. A CW laser beam (F-number=1.6) propagates along the symmetry z axis, with its focal point at the ellipse center. The initial arc plasma is described by a Gaussian temperature profile (maximum 8000 K). The model assumes local thermal equilibrium, coupling the conservation equations for mass, momentum and energy with a partial differential equation (PDE) based on Lambert-Beer's law for laser absorption. The governing equations are solved self-consistently using the finite-element method in COMSOL, with a hybrid mesh refined around the plasma core.

RESULTS AND DISCUSSION

Periodical oscillations in LSP brightness

Figure 2(a) present the temporal brightness signals of the LSP obtained from photodetector measurements and

numerical simulation, respectively. The analog voltage from the detector captures the luminous fluctuations of LSP, while the simulated signal is derived from the domain-integrated radiative power. Their corresponding frequency spectra, obtained via FFT, are shown in Fig. 2(b), where the solid lines represent experimental results, and the dashed line denotes simulated ones. The oscillation frequency f_{os} ranges from 24 to 28 Hz across 300-600 W laser power in both cases. The overall discrepancy between simulations and experiments is below 5% [Fig. 2(c)], validating our simulation model.

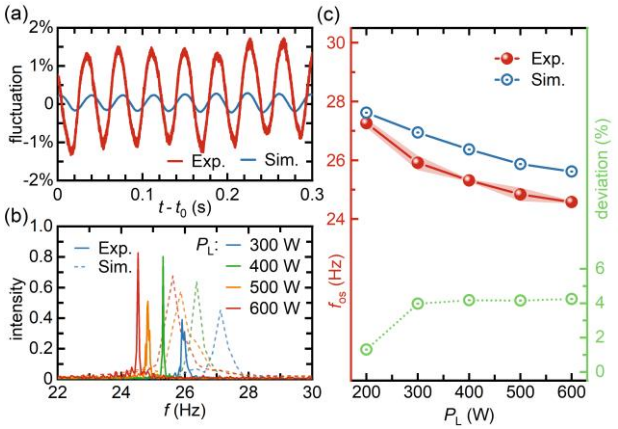

Figure 2: (a) Time-dependent LSP brightness signal obtained from experiments and simulation. (b) Spectrograms derived via FFT from experiment and simulation results. (c) Comparison of f_{os} between the experiments and simulations.

Vortex evolution around the LSP core

Figure 3(a) presents shadow images capturing one oscillation period of the LSP under 200 W laser power. Bright lines in the images correspond to regions with a maximum second spatial derivative of density $\nabla^2\rho/\nabla z^2$, outlining the bubble-shaped boundary between the hot plume and the cooler surrounding gas. A bubble forms at $t = T_{os}/4$, and then expands and rises. Obstruction by the anode leads to an accumulation of floating gas, forming an inversion layer where denser gas overlies the lighter gas. This configuration triggers a Rayleigh-Taylor instability, and strong velocity shear then induces a Kelvin-Helmholtz instability, resulting in vortex roll-up and a transition to turbulence. By the end of the period ($t = T_{os}$), the bubble replicates the initial morphology and confirming the periodic nature. Figure 3(b) shows distributions of vorticity $\boldsymbol{\omega} = \nabla \times \mathbf{u}$ (left) and velocity $\mathbf{u}$ streamlines (right). Vorticity concentrates in a thin elliptical boundary layer around the core. A toroidal vortex periodically forms on this shear layer, as seen in gray streamlines. The cyclic vortex ring formation, development, floating, and detachment processes cause periodic changes in LSP core shape and size. This instability results in sinusoidal luminous intensity variations, as shown in Fig. 3(c).

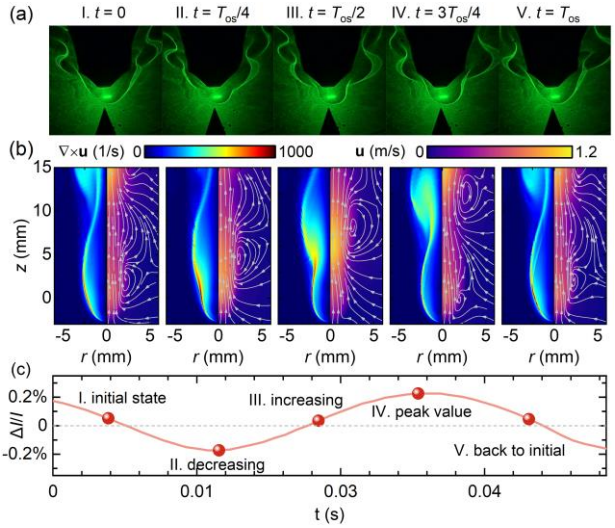

Figure 3: (a) Shadow images of the LSP plume at different stages. (b) Distributions of vorticity (left columns) and the vortex evolution in one oscillation period. (c) Fluctuation of the LSP radiation power in the corresponding period.

Scaling law for LSP oscillation frequency

Figure 4(a) illustrates the fundamental processes in LSP, including laser absorption, radiation, buoyancy -driven convection, and thermal diffusion. A focused laser creates steep temperature and density gradients, causing the hot core to rise via buoyancy. This upward flow generates velocity shear and vortices along its boundary. Concurrently, thermal diffusion dissipates heat outward, reducing these gradients. The characteristic LSP oscillation frequency is thus determined by the competition between buoyant acceleration (promoting vortex motion) and thermal diffusion (suppressing it).

Guided by the mechanism above, we propose a new theoretical expression for the LSP oscillation frequency f_B, incorporating buoyant acceleration a_{bou} and thermal diffusivity α_{dif} as the key competing terms, which is

$$f_B = F\ (\sigma_{den}, g, C_p, k_T, \rho) = F\ (a_{bou}, \alpha_{dif}), \qquad (1)$$

where $\sigma_{den} = \rho_{out}/\rho_{in}$ is the ratio between the ambient gas density ρ_{out} and the LSP plume density ρ_{in}, g is the gravitational acceleration; C_p, k_T, and ρ are the specific capacity, thermal conductivity, and mass density of gas.

We perform a dimensional analysis of the new scaling law in Eq. (1) based on the Buckingham Π-theorem [7]. Four independent fundamental units are used: mass [M] = kg, length [L] = m, time [T] = s, and temperature [Θ]=K. The dimensions of the relevant physical quantities are: $f_B \sim [T^{-1}]$, $g \sim [LT^{-2}]$, $C_p \sim [L^2T^{-3}\Theta^{-1}]$, $k_T \sim [MLT^{-4}\Theta^{-1}]$, and $\rho \sim [ML^{-3}]$. According to the Π-theorem, a dimensionless group is formed as:

$$\Pi = \frac{f_B}{C_p^{\lambda_1} k_T^{\lambda_2} g^{\lambda_3} \rho^{\lambda_4}}. \quad (2)$$

Applying dimensional homogeneity for [M], [L], [T], and [Θ] leads to the following equations:

$$\begin{bmatrix} M \\ L \\ T \\ \Theta \end{bmatrix} : \begin{bmatrix} 0 & 1 & 0 & -1 \\ 2 & 1 & 1 & -3 \\ -3 & -4 & -2 & 1 \\ -1 & -1 & 0 & 0 \end{bmatrix} \begin{bmatrix} \lambda_1 \\ \lambda_2 \\ \lambda_3 \\ \lambda_4 \end{bmatrix} = \begin{bmatrix} 0 \\ 0 \\ -1 \\ 0 \end{bmatrix}, \quad (3)$$

solving this yields $\lambda_1 = 1/3$, $\lambda_2 = -1/3$, $\lambda_3 = 2/3$, and $\lambda_4 = 1/3$. Assuming the dimensionless parameter σ_{den} scales with the same power as g, the theoretical f_B is expressed as

$$f_B \propto \left[\frac{C_p (\sigma_{den} - 1)^2 g^2 \rho}{k_T} \right]^{1/3} = \left(\frac{a_{bou}^2}{\alpha_{dif}} \right)^{1/3}. \quad (4)$$

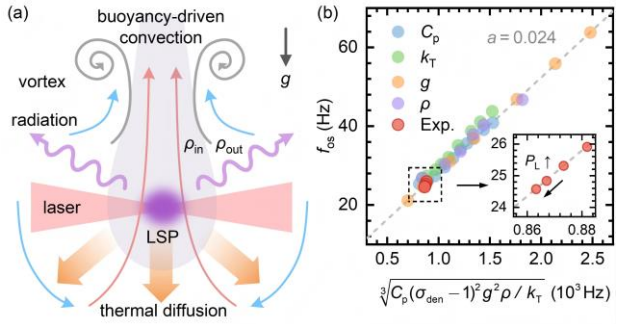

Figure 4: (a) Mass and energy transport processes in LSP. (b) Scaling relation between the measured f_{os} and theoretical f_B. Experimental measurements (red circles) are obtained by tuning the input laser power [8].

Figure 4(b) shows the measured f_{os}, scales linearly with the theoretical prediction f_B from Eq. (4). Data were acquired by systematically varying the normalized parameters in simulations, with normalization relative to a baseline case (16 atm Xe, g = 9.8 m/s^2, input laser power P_L = 500 W). The measured f_{os} values align closely with f_B, confirming the proposed linear scaling relation.

Two mechanisms of tuning LSP oscillation frequency

The scaling law indicates that the LSP oscillation dynamics are governed by a balance between buoyancy -driven acceleration—which promotes vortex stretching and shedding—and thermal diffusion, which acts to relax temperature and density gradients. Figure 5 illustrates the mechanisms that the control parameters regulate the vortex dynamics and LSP oscillation frequency. An increase in (C_p, ρ) or a decrease in k_T reduces the thermal diffusivity α_{dif}, which compresses the shear layer and thereby decreases the vortex detachment height h_d. Conversely, an increase in the gravitational acceleration g enhances the buoyant acceleration a_{buo} and the vorticity evolution rate Dω/Dt, leading to a higher vortex rising speed u_ω. These two distinct tuning mechanisms operate synergistically to determine f_{os} according to $f_{os} \sim u_\omega / h_d$.

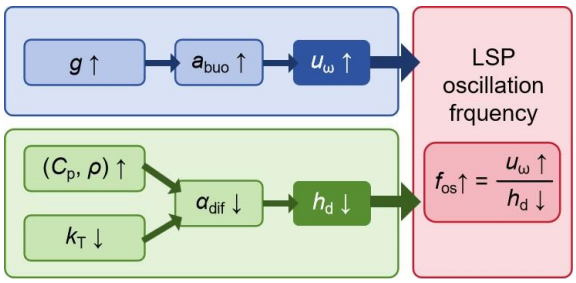

Figure 5: Modulation mechanisms of the parameters on the vortex dynamics and LSP oscillation frequency.

CONCLUSION

This combined experimental and computational study establishes scaling laws for LSP oscillations, revealing their governing buoyancy-driven vortex dynamics. Buoyancy induced by temperature gradient drives periodic vortex formation, growth, and detachment, directly dictating LSP brightness and shape fluctuations. We derive the scaling relation $f_{os} \propto [(\sigma_{den}-1)^2 C_p g^2 \rho / k_T]^{1/3}$, indicating that f_{os} is set by the competition between thermal diffusivity (governing vortex detachment height) and gravitational acceleration (setting vortex rise speed). This framework advances the prediction of LSP dynamics and provides practical guidance for enhancing LSP stability in optical inspection systems.

ACKNOWLEDGEMENTS

The authors acknowledge the financial support from the Organized Research Support Program (No. YK20240103) from the Department of Electrical Engineering at Tsinghua University, the National Natural Science Foundation of China (No. 52277154), and the Beijing Natural Science Foundation (No. 3244040).

REFERENCES

[1] D. Zhang, J. Liu, and Y. Fu, Phys. Rev. Appl., vol. 23(5), 2025, p. 054083.

[2] Z. Shi, S. Yang, H. Hu, H. Lei, Z. Yang, and X. Yu, Light Sci. Appl., vol. 13, 2024, p. 274.

[3] M. A. Kotov, S. Y. Lavrentyev, A. N. Shemyakin, N. G. Solovyov, and M. Y. Yakimov, Plasma Sources Sci. Technol., vol. 31, 2022, p.124002.

[4] H. Hu, S. Yang, Z. Shi, and X. Yu, Opt. Laser Technol., vol. 189, 2025, p. 113098.

[5] D. Zhang, J. Liu, and Y. Fu, Acta Phys. Sin., vol. 73(2), 2024, p. 025201.

[6] D. Zhang, J. Mao, P. Zhang, J.P. Verboncoeur, and Y. Fu, Phys. Rev. Fluids, under review.

[7] E. Buckingham, Phys. Rev., vol. 4(4), 1914, p.345.

[8] D. Zhang, J. Mao, and Y. Fu, Phys. Rev. Appl., under review.